Temporal coupled-mode theory for resonant apertures

Lieven Verslegers,[1,*] Zongfu Yu,[1] Peter B. Catrysse,[1] and Shanhui Fan[1,2]

[1]*E. L. Ginzton Laboratory and Department of Electrical Engineering, Stanford University, Stanford, California 94305, USA*
[2]*e-mail: shanhui@stanford.edu*
**Corresponding author: lievenv@stanford.edu*

Received July 7, 2010; accepted July 24, 2010;
posted August 2, 2010 (Doc. ID 130986); published September 9, 2010

We develop the coupled-mode theory for nanoscale resonant apertures. We show that the maximum transmission and absorption cross sections for subwavelength resonant apertures are only related to the wavelength of the incident light and the directivity of the aperture's radiation pattern. A general relation between the transmission cross section and the directivity is proven from the coupled-mode theory. As a specific example, we apply the theory to a nanoslit aperture in a metallic film and obtain excellent agreement with direct numerical simulations.

OCIS codes: 050.1220, 260.5740, 310.6628, 260.3910, 240.6680.

1. INTRODUCTION

Absorption, scattering, and extinction cross sections are concepts that are fundamentally important for characterizing electromagnetic properties of individual objects [1]. These concepts are now being applied in nanophotonics to individual nanoparticles [2–4], including individual split ring resonators [5], and optical antennas [6].

Following the observation of strongly enhanced transmission of light through arrays of subwavelength holes in metallic films [7], there has been a tremendous amount of research on nanoscale apertures [8–10]. Such apertures are of fundamental interest and form the basic building blocks for many applications in subwavelength optics and optoelectronics. The transmission cross section of an individual aperture, to an extent the dual of the extinction cross section of a nanoparticle, has been calculated [11–15] and experimentally measured [11,16] for specific geometries.

In contrast to the existing detailed numerical and experimental works on individual apertures, here we aim to illustrate some of the general aspects of the transmission and absorption cross sections of resonant apertures with the use of the temporal coupled-mode theory (CMT). The temporal CMT provides a general framework for the study of many optical devices [17]. In optics, the temporal CMT is mostly used to describe coupling between resonant cavities and discrete propagating waveguide modes. Due to its generality, it reduces the understanding of a complex system to a few parameters. Recently, the temporal CMT has also been applied to the free-space resonant scattering of waves [18,19]. References [18,19], however, only consider scatterers that have certain cylindrical or spherical symmetry, or are small compared to the wavelength. In this paper, we extend the use of the temporal CMT for calculations of cross sections of objects without rotational symmetry.

To illustrate our theory, we focus on the simplest of apertures: the slit. Previously slits have been studied extensively, using modal expansion techniques and numerical simulations, and their transmission properties have been characterized experimentally [11,20–26]. On the application side, nanostructured metallic devices based on slits have been shown to achieve highly directional emission [27], enhanced transmission [11,28,29], and controlled focusing [30–36], as well as improved photodetection (absorption) [37,38]. The theory we set forth applies to slits, but equally well to the general case of a resonant aperture.

In our theory, an aperture is treated as a resonance (or multiple resonances at different frequencies). The approach is analytical and, depending on the application, can account for directivity, surface plasmon excitation, and material absorption. The theory demonstrates that the maximum transmission and absorption cross sections are only related to the wavelength of the incident light and directivity of the aperture's radiation pattern. Such an understanding should be beneficial for the design and optimization of new optical components.

For the case of the slit, part of our theory constitutes a reformulation of antenna theory and the concept of an effective area [39,40]. Indeed, a slit in a metallic film can be considered as an aperture antenna coupled to a similar antenna through a transmission line. In fact, concepts from radiofrequency theory have already been used to improve nanoantennas [41]. We opt to cast our theory in a language more common and suitable for optics.

In Section 2, we develop the CMT, from which we derive the transmission cross section for the isotropic radiator (Subsection 3.A) and the anisotropic radiator (Subsection 3.B). In Subsection 3.C we introduce a relation between transmission cross section and wavelength. Subsection 3.D treats the effect of the excitation of surface

plasmons; Subsection 3.E deals with material absorption in resonant apertures. In Section 4, we derive the absorption cross section. Finally, we conclude in Section 5.

2. TEMPORAL COUPLED-MODE THEORY

To illustrate the theory, we study a single slit in a metallic film as a concrete implementation of a resonant aperture (Fig. 1). We consider the whole structure in two dimensions and light with transverse magnetic (TM) polarization (E_x,H_y,E_z). For the TM polarization, the slit supports a propagating mode no matter how small is its width. A resonance can then be formed due to the reflections of such a propagating mode at the entrances to the slit. As a result, the slit can be treated as a resonator coupled to free space on both sides [23]. We consider a single resonance first. The complex amplitude of the resonator mode is denoted by A, with $|A|^2$ describing the energy inside the slit.

The CMT describes the interaction between such resonances with the surrounding environment. The surrounding environment is described by channels that carry incoming and outgoing waves with respect to the resonance [42]. For a given channel, the amplitudes of incoming and outgoing waves are described by s_+ and s_-, respectively, with $|s|^2$ representing the power in the wave.

Depending on the model used for the metal there can be different types of channels. One type of channel that is always present consists of plane waves propagating in free space in different directions. We distinguish between plane waves that are above (labeled by a subscript T) or below (labeled by a subscript B) the film. Also, to facilitate the description of these plane wave channels, we impose a periodic boundary condition with period L (Fig. 2, inset). In this way the channels become discrete (Fig. 2) and can in addition be labeled with respect to the parallel wave vector components of $2\pi n/L$, with n being integers. With these subscripts, a wave incident from the top half-space onto the slit, having a parallel wave vector $2\pi n/L$, for example, has its amplitude labeled as $s_{T,n+}$. Moreover, since these are propagating waves, we have

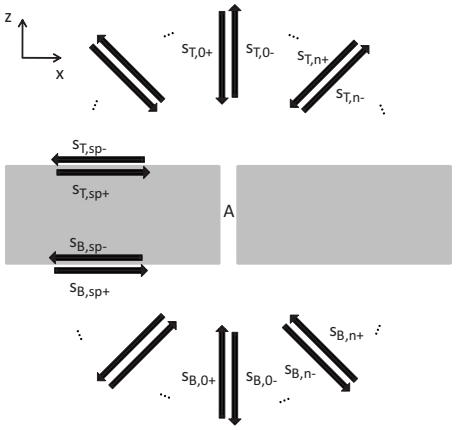

Fig. 1. CMT of a slit in an optically thick metallic film. The slit couples with free-space channels above (with amplitudes $s_{T,n+}$ and $s_{T,n-}$) and below (with amplitudes $s_{B,n+}$ and $s_{B,n-}$) the film, as well as with the surface plasmon channels (with amplitudes $s_{T,sp+}$, $s_{T,sp-}$, $s_{B,sp+}$, and $s_{B,sp-}$). The channels are shown as discrete modes.

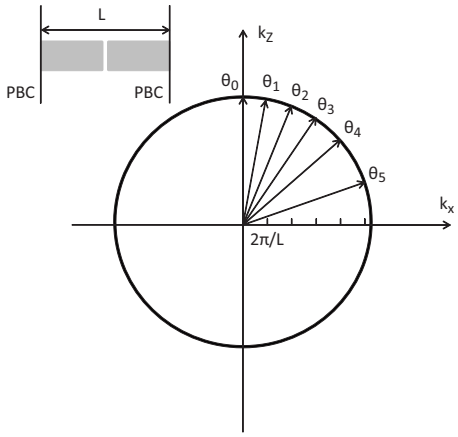

Fig. 2. Channels in k space for a slit in a metallic film with periodic boundary condition (PBC). k_x and k_z are the spatial frequencies in the x and z directions. The CMT explicitly makes the conversion from discrete modes to a continuous spatial spectrum by assuming a periodic boundary condition and letting the spatial period L, and consequently N, go to infinity at the end of the calculation. Under this assumption, channels are equally spaced in spatial frequency k_x, but not in angle.

$$|n| \le N \equiv \left\lfloor \frac{\omega_0 L}{2\pi c} \right\rfloor = \left\lfloor \frac{L}{\lambda_0} \right\rfloor, \tag{1}$$

where ω_0 (λ_0) is the resonant frequency (wavelength) and c is the speed of light. Thus the total number of channels, N, in free space is finite. We take the limit $L \to \infty$ to recover the case of a single slit with a continuum of plane wave channels.

When the metal is plasmonic, there is a second type of channels (labeled by a subscript sp) consisting of plasmonic surface modes on the top and bottom metal-air interfaces. The amplitudes of these channels at the top and bottom metal-air interfaces are given as $s_{T,sp+}$, $s_{T,sp-}$, $s_{B,sp+}$, and $s_{B,sp-}$. Note that here we combine the surface plasmon channels to the left and the right of the slit. In analyses that focus more specifically on surface plasmon generation, they could be split up.

We first consider a plane wave normally incident on the slit, as described by an amplitude $s_{T,0+}$. In this case, since there is no incident wave in other channels, the relevant temporal coupled-mode equations can be written as [17,42,43]

$$\frac{dA}{dt} + \left(-i\omega_0 + \sum_{n=-N}^{N} \gamma_{T,n} + \sum_{n=-N}^{N} \gamma_{B,n} + \gamma_{T,sp} + \gamma_{B,sp} + \gamma_a \right) A = \sqrt{2\gamma_{T,0}} s_{T,0+}, \tag{2}$$

$$s_{B,n-} = \sqrt{2\gamma_{B,n}} A, \tag{3}$$

$$s_{B,sp-} = \sqrt{2\gamma_{B,sp}} A. \tag{4}$$

Here $\gamma_{T,n}$, $\gamma_{B,n}$, $\gamma_{T,sp}$, and $\gamma_{B,sp}$ are the amplitude leakage rates with which the slit mode couples to the free space and surface plasmon channels. We also include an intrinsic amplitude loss rate γ_a for the resonance.

Equations (2)–(4) allow us to solve for the transmission spectrum $T(\omega)$:

$$T(\omega)=\frac{\sum_{n=-N}^{N}|s_{B,n-}|^2+|s_{B,sp-}|^2}{|s_{T,0+}|^2}=\frac{2\gamma_{T,0}\left(2\sum_{n=-N}^{N}\gamma_{B,n}+2\gamma_{B,sp}\right)}{(\omega-\omega_0)^2+\left(\sum_{n=-N}^{N}\gamma_{T,n}+\sum_{n=-N}^{N}\gamma_{B,n}+\gamma_{T,sp}+\gamma_{B,sp}+\gamma_a\right)^2}=\frac{2\gamma_0\left(2\sum_{n=-N}^{N}\gamma_n+2\gamma_{sp}\right)}{(\omega-\omega_0)^2+\left(2\sum_{n=-N}^{N}\gamma_n+2\gamma_{sp}+\gamma_a\right)^2}. \tag{5}$$

In the last step of the derivation we used the fact that the setup is symmetric for top/bottom and set $\gamma_n=\gamma_{B,n}=\gamma_{T,n}$ and $\gamma_{sp}=\gamma_{B,sp}=\gamma_{T,sp}$. Henceforth, we leave out subscripts for top and bottom. At any frequency, the transmission coefficient $T(\omega)$ takes on a value between 0 and 1. For off-normal incidence, as described by excitation of the slit through channel $s_{T,m+}$, with angle θ_m to the normal, the transmission coefficient can similarly be calculated as

$$T(\omega,\theta_m)=\frac{2\gamma_m\left(2\sum_{n=-N}^{N}\gamma_n+2\gamma_{sp}\right)}{(\omega-\omega_0)^2+\left(2\sum_{n=-N}^{N}\gamma_n+2\gamma_{sp}+\gamma_a\right)^2}. \tag{6}$$

3. TRANSMISSION CROSS SECTION

The transmission spectrum $T(\omega)$, as defined in Eq. (5), is not very meaningful in the case of a single slit since it depends on the choice of L, as defined by the artificial periodic boundary condition. In this section, we will take the limit of $L\to\infty$ in order to calculate the transmission cross section of a single slit. For a single slit, the transmission cross section $\sigma_T(\omega)$ is defined as the ratio between the total transmitted power and the intensity of an incident plane wave [44]. It has a dimension of length for our two-dimensional case. In the formalism here, for normal incidence, we will therefore calculate

$$\sigma_T(\omega)=\frac{\sum_{n=-N}^{N}|s_{B,n-}|^2+|s_{B,sp-}|^2}{|s_{T,0+}|^2/L}=T(\omega)L, \tag{7}$$

in the limit where $L\to\infty$. For off-normal incidence through channel m, the transmission cross section becomes

$$\sigma_T(\omega,\theta_m)=\frac{\sum_{n=-N}^{N}|s_{B,n-}|^2+|s_{B,sp-}|^2}{|s_{T,m+}|^2/(L\cos\theta_m)}=T(\omega,\theta_m)L\cos\theta_m. \tag{8}$$

The factor $\cos\theta_m$ appears because the intensity of the wave in the mth channel is $|s_{T,m+}|^2/(L\cos\theta_m)$.

A. Isotropic Radiation

First, we evaluate the transmission cross section of a resonant aperture with an isotropic radiation pattern. This means that radiation emitted from the aperture has an equal intensity in all directions outside the metal film. An example of such an aperture is a deep-subwavelength slit in a perfect electrical conductor (PEC) film [20]. In this case, the surface plasmon channels and material loss are absent, and we consider only those channels that are propagating waves in free space.

With our use of a periodic boundary condition, the channels provide a uniform sampling of the parallel wave vector space. As can be seen from Fig. 2, these channels therefore do not provide a uniform sampling of the angular space. In order to describe an isotropic radiator, the coupling constant γ_n for the nth channel at angle θ_n needs to be set to be proportional to its associated arc $\Delta\theta_n=\Delta(\sin\theta_n)/\cos\theta_n=1/N\cos\theta_n$. For an isotropic radiator, the leakage rate to the nth channel γ_n is then related to the leakage rate in the normal direction as

$$\gamma_n=\frac{\gamma_0}{\cos\theta_n}. \tag{9}$$

The total radiative rate to the free-space modes above (below) the film in the $L\to\infty$ limit is therefore

$$\sum_{n=-N}^{N}\gamma_n=\gamma_0\sum_{n=-N}^{N}\frac{1}{\cos\theta_n}=N\pi\gamma_0. \tag{10}$$

Using Eqs. (1), (6), and (8)–(10), the transmission cross section spectrum simplifies to

$$\sigma_{T,\mathrm{isotropic}}(\omega,\theta_m)=\frac{2\gamma_m L\cos\theta_m\left(2\sum_{n=-N}^{N}\gamma_n\right)}{(\omega-\omega_0)^2+\left(2\sum_{n=-N}^{N}\gamma_n\right)^2}=\frac{2\gamma_0 L\left(2\sum_{n=-N}^{N}\gamma_n\right)}{(\omega-\omega_0)^2+\left(2\sum_{n=-N}^{N}\gamma_n\right)^2}=\frac{\lambda_0}{\pi}\frac{\frac{1}{4Q^2}}{\left(\frac{\omega-\omega_0}{\omega_0}\right)^2+\frac{1}{4Q^2}}, \tag{11}$$

where, following the standard definition, the quality factor Q is the ratio between the resonant frequency and the full width at half-maximum of the resonance line shape:

$$Q = \frac{\omega_0}{\frac{N}{4\sum_{n=-N}\gamma_n}}. \quad (12)$$

From Eq. (11), we see that the spectrum has a Lorentzian line shape, and that the transmission cross section reaches a maximum of

$$\sigma_{T,\text{isotropic}}(\omega_0, \theta_m) = \frac{\lambda_0}{\pi} \quad (13)$$

at the resonant frequency. For the isotropic aperture, the cross section is also isotropic in the sense that it does not depend on the angle of incidence. The maximal transmission cross section scales linearly with the wavelength of the incident light. Moreover, it is independent of the slit width and can thus be much larger than the aperture's geometric cross section. The derivation that we presented above is straightforwardly generalized to the three-dimensional case of the resonant aperture coupling two half-spaces (Appendix A).

We now verify the theory with finite-difference frequency-domain (FDFD) simulations [45] of a 150 nm narrow slit in a 1 μm thick film made of a PEC. We first verify that such a slit indeed behaves as an isotropic radiator. To generate the radiation pattern, we excite the structure by placing a source inside the slit and generate a contour plot [Fig. 3(b)] of the resulting magnetic field intensity in the free space. The contours are to a good approximation circular, confirming isotropic radiation.

To calculate the transmission cross section, we excite the structure with a normally incident plane wave and calculate the total transmitted power at the exit surface of the slit. The transmission cross section $\sigma_T(\omega)$ is then obtained by normalizing such transmitted power with respect to the incident flux. The blue dots in Fig. 3(a) show the simulated transmission cross section as a function of wavelength. The transmission cross section is normalized over the slit width to give a measure of the enhancement.

We compare the simulated cross section with the theory as outlined above. The simulated cross section indicates that the structure supports multiple resonances. We describe the cross section of the ith resonance using Eq. (11), with a quality factor Q_i. Since these resonances are spectrally well separated, we take into account the effect of multiple resonances by summing over the cross sections $\sigma_{T,i}(\omega)$ of all resonances. As a result

$$\sigma_T(\omega) = \sum_i \frac{\lambda_{0,i}}{\pi} \frac{\frac{1}{4Q_i^2}}{\left(\frac{\omega-\omega_{0,i}}{\omega_{0,i}}\right)^2 + \frac{1}{4Q_i^2}} = \sum_i \sigma_{T,i}(\omega). \quad (14)$$

Theory [green curve in Fig. 3(a)] and simulations are found to be in good agreement. In particular, the peak transmission cross section can be well approximated by the maximal transmission cross section (λ/π) of a single isotropic radiator [red line in Fig. 3(a)]. The simulation thus provides a direct confirmation of the analytical theory. Note that the CMT is a theory of resonances. It should in principle only be valid in the vicinity of the individual resonances, and individual resonances can be added if they are spectrally sufficiently separated. We find empirically that summing the resonances gives a good idea of the global spectral behavior.

B. Anisotropic Radiation and Directivity

For a single resonant aperture, it is possible to achieve a transmission cross section that goes beyond the limit of λ/π for the isotropic case by creating anisotropy in the radiation pattern [11,27,28]. This can be done, for instance, by introducing surface corrugation (Fig. 4) or by modifying the entrances to the slits (Fig. 5).

To illustrate that our formalism also describes such anisotropic cases, we start by calculating the transmission cross section for normally incident light. For this purpose, we define the directivity D in the normal direction (in the $N\to\infty$ limit) [46]:

$$D = \frac{\gamma_0 N\pi}{\frac{N}{\sum_{n=-N}\gamma_n}}. \quad (15)$$

The higher the leakage rate to channel 0, the more normally directional the structure will be. The theory then incorporates directivity as follows:

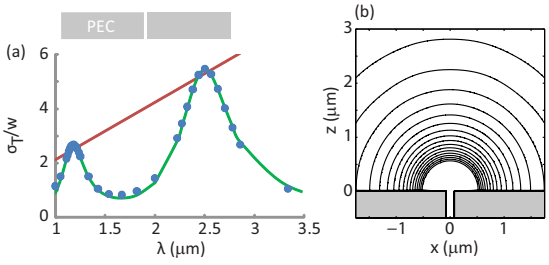

Fig. 3. (Color online) Single slit in a PEC. (a) The theoretical normalized transmission cross section spectrum (green curve) and from FDFD simulations (blue dots). The straight red line indicates the maximal transmission cross section of an isotropic radiator. (b) Contour plot of the magnetic field intensity for the single slit excited at 1.176 μm.

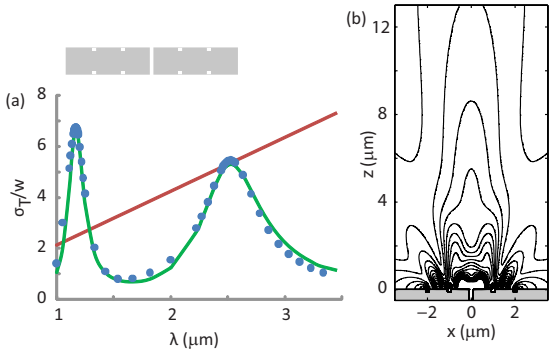

Fig. 4. (Color online) Slit with surface corrugation. (a) The theoretical normalized transmission cross section spectrum (green curve) and from FDFD simulations (blue dots). The straight red line shows the maximal transmission cross section of an isotropic radiator. (b) Contour plot of the magnetic field intensity for the structure excited at 1.168 μm shows directional emission.

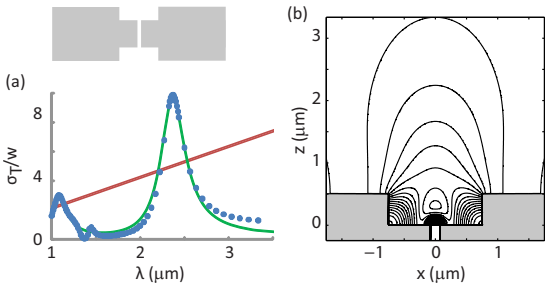

Fig. 5. (Color online) Slit with wider slits at its ends. (a) The theoretical normalized transmission cross section spectrum (green curve) and from FDFD simulations (blue dots). The straight red line shows the maximal transmission cross section of an isotropic radiator. (b) Contour plot of the magnetic field intensity for the structure excited at 2.370 μm shows directional emission.

$$\sigma_T(\omega) = \frac{D\lambda_0}{\pi} \frac{\frac{1}{4Q^2}}{\left(\frac{\omega-\omega_0}{\omega_0}\right)^2 + \frac{1}{4Q^2}} = D\sigma_{T,\text{isotropic}}(\omega). \quad (16)$$

This result can be easily generalized for other directions. By defining an angle-dependent directivity,

$$D(\theta_m) = \frac{\gamma_m N\pi \cos(\theta_m)}{\sum_{n=-N}^{N} \gamma_n}, \quad (17)$$

we obtain the transmission cross section for light incident at an angle θ_m:

$$\begin{aligned}\sigma_T(\omega,\theta_m) &= T(\omega,\theta_m)L\cos(\theta_m)\\ &= \frac{2\gamma_m L\cos(\theta_m)\left(2\sum_{n=-N}^{N}\gamma_n\right)}{(\omega-\omega_0)^2 + \left(2\sum_{n=-N}^{N}\gamma_n\right)^2}\\ &= \frac{D(\theta_m)\lambda_0}{\pi}\frac{\frac{1}{4Q^2}}{\left(\frac{\omega-\omega_0}{\omega_0}\right)^2+\frac{1}{4Q^2}} = D(\theta_m)\sigma_{T,\text{isotropic}}(\omega).\end{aligned} \quad (18)$$

For an anisotropic radiator, an increased directivity for radiation in a certain direction is directly related to the enhanced transmission cross section for light coming in from that direction. From Eq. (17) it is clear that there exists a trade-off between a large transmission cross section and a large angular range of operation.

We now confirm the theory developed in the previous paragraphs through numerical simulations. For this purpose we consider two different structures (Figs. 4 and 5). The structure in Fig. 4 consists of the same slit in the PEC as in Fig. 3 with a width of 150 nm. The slit is placed in the middle of an array of grooves 150 nm wide and 120 nm deep, spaced 1 μm apart. For the structure in Fig. 5, we instead modify the entrance and exit ends of the 150 nm wide slit by placing slits that are 1.5 μm wide and 0.5 μm deep at both ends.

We obtain the directivities at resonant wavelengths for both structures in Figs. 4 and 5 from simulations. We excite the mode inside the slit and generate the radiation pattern. A far-field flux F_{FF} over one grid point Δx, at a distance z_{FF} directly above the slit, is then compared to the total flux emitted, F_{tot}, to obtain the directivity $D = F_{\text{FF}} z_{\text{FF}} \pi / (F_{\text{tot}} \Delta x)$. We choose the distance z_{FF} to be sufficiently far, i.e., in such a way that the numerically determined directivity becomes independent of z_{FF}. The transmission cross section of the structure at normal incidence is obtained in the same way as the case in Fig. 3.

The transmission cross sections of both structures in Figs. 4 and 5 exhibit resonance with peak transmission cross sections well beyond λ/π [at $\lambda = 1.168$ μm in Fig. 4(a) and at $\lambda = 2.370$ μm in Fig. 5(a)]. At the peak wavelengths of these resonances, the radiation patterns [Figs. 4(b) and 5(b)] show strong anisotropy, with stronger radiation in the normal direction. The theoretical cross section spectra in the vicinity of these resonances, with the directivity obtained from simulations ($D = 2.67$ at $\lambda = 1.168$ μm and $D = 1.91$ at $\lambda = 2.370$ μm), agree quite well with the direct numerical simulation of the cross section of the structure. The simulations thus provide a direct confirmation of the mechanism for enhancing the cross section by way of achieving a stronger directivity.

C. Angular Sum Rule for the Peak Transmission Cross Section

The previous results also allow us to derive a general sum rule regarding the peak resonant transmission cross section of a single resonance:

$$\begin{aligned}\int_{-\pi/2}^{\pi/2}\sigma_T(\omega_0,\theta)d\theta &= \sum_{m=-N}^{N}\sigma_T(\omega_0,\theta_m)\frac{1}{N\cos\theta_m}\\ &= \frac{\lambda_0}{\pi}\sum_{m=-N}^{N}D(\theta_m)\frac{1}{N\cos\theta_m}\\ &= \frac{\lambda_0}{\pi}\sum_{m=-N}^{N}\frac{\gamma_m\pi}{\sum_{n=-N}^{N}\gamma_n} = \lambda_0.\end{aligned} \quad (19)$$

This relation is equally valid for anisotropic and isotropic radiators. This sum rule summarizes, in a very compact fashion, the trade-off between directivity and transmission cross section as discussed in detail in Subsection 3.B. It is important to note here that the concept of directivity is related to the existence of a single resonance. If multiple resonances are present, radiation pattern and directivity can no longer be unambiguously defined since these then depend on the phase and amplitude excitation of the resonances.

D. Surface Plasmons

We now consider the case of a single slit aperture in a plasmonic metal. In contrast to the case considered above, where the metal is a PEC, with a plasmonic metal there exist surface plasmon modes at the top and bottom surfaces of the metal film. These surface plasmon modes provide additional channels that the resonance in the slit can couple into. Taking into account the contribution from the additional surface plasmon channels, the transmission cross section of the slit in the presence of normally incident light can be derived as

$$\sigma_T(\omega) = \frac{2\gamma_0 L\left(2\sum_{n=-N}^{N}\gamma_n + 2\gamma_{sp}\right)}{(\omega-\omega_0)^2 + \left(2\sum_{n=-N}^{N}\gamma_n + 2\gamma_{sp}\right)^2}$$

$$= \frac{\frac{2\gamma_0 L}{N}\left(2\sum_{n=-N}^{N}\gamma_n + 2\gamma_{sp}\right)^2}{2\sum_{n=-N}^{N}\gamma_n + 2\gamma_{sp}} \Big/ \left[(\omega-\omega_0)^2 + \left(2\sum_{n=-N}^{N}\gamma_n + 2\gamma_{sp}\right)^2\right]$$

$$= \frac{D\lambda_0}{\pi}\frac{\frac{2\sum_{n=-N}^{N}\gamma_n}{N}\left(2\sum_{n=-N}^{N}\gamma_n + 2\gamma_{sp}\right)^2}{2\sum_{n=-N}^{N}\gamma_n + 2\gamma_{sp}} \Big/ \left[(\omega-\omega_0)^2 + \left(2\sum_{n=-N}^{N}\gamma_n + 2\gamma_{sp}\right)^2\right]$$

$$= \frac{G\lambda_0}{\pi}\frac{\frac{1}{4Q^2}}{\left(\frac{\omega-\omega_0}{\omega_0}\right)^2 + \frac{1}{4Q^2}} = G\sigma_{T,\text{isotropic}}(\omega), \quad (20)$$

with G defined as [47]

$$G = \frac{2\sum_{n=-N}^{N}\gamma_n}{2\sum_{n=-N}^{N}\gamma_n + 2\gamma_{sp}} D = e_r D, \quad (21)$$

and

$$Q = \frac{\omega_0}{4\left(\sum_{n=-N}^{N}\gamma_n + \gamma_{sp}\right)}. \quad (22)$$

In Eq. (21) D is the directivity that characterizes the radiation pattern of an antenna. It is defined the same as before [Eq. (15)]. In the presence of surface plasmon channels, Eq. (21) shows that, in addition to the directivity, the transmission cross section is now also related to the radiation efficiency e_r, which for a radiating antenna is the ratio between the radiated power and the input power.

In the presence of surface plasmon channels, our theory therefore shows that the transmission cross section will be lowered for the *single* aperture since the surface plasmon acts as a loss channel. This is in contrast with the extensively studied phenomenon of extraordinary transmission [7–10], which occurs in *arrays* of apertures, and generally results from the evanescent leakage of a surface resonance through the holes.

To compare theory to simulation, we consider the case of a slit in a gold film [Fig. 6(a)]. To illustrate the theory in the absence of the material loss, here we describe gold using only the real part of its tabulated dielectric constant [48]. We obtain the values of G from simulations at the resonant wavelengths. We excite the slit and measure the total flux delivered to the aperture, F_{tot}. This flux line is placed inside and perpendicular to the slit, at 0.5 μm from the exit plane, in order to include the part of the power delivered to the surface plasmon channel inside the metal film. We then find the flux F_{FF} over a line that is one grid point Δx long, at a distance z_{FF}, directly above the slit, in the far field. This leads to $G = F_{\text{FF}} z_{\text{FF}} \pi / (F_{\text{tot}} \Delta x)$. The simulated values for G at 2.857, 1.367, 0.893, and 0.676 μm are, respectively, 0.96, 0.92, 0.88, and 0.83.

Since the surface plasmon excitation is most prominent at the shorter wavelengths, we will focus on the peak at 0.676 μm [Fig. 6(b)]. The numerically obtained transmission cross section agrees quite well with Eq. (20) using the G factor as obtained numerically above. At this wavelength, due to the penetration into the metal, the slit appears wider and has a higher directivity than the corresponding PEC case, which enhances the cross section at normal incidence. The surface plasmon channel, on the other hand, provides an additional leakage channel that reduces the cross section. As a result of these two conflicting trends, for this particular structure, the assumption of a more realistic plasmonic metal model has led to a lower transmission cross section.

E. Absorption

The general theory of the resonance [Eq. (2)] includes a loss channel, with loss rate γ_a, resulting from material absorption. In the presence of material loss, the transmission cross section of a single resonance is

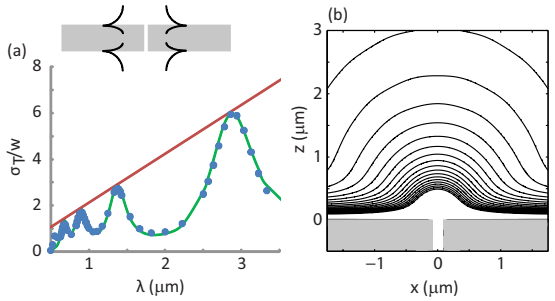

Fig. 6. (Color online) Single slit in real metal (gold). (a) The theoretical normalized transmission cross section spectrum (green curve) and from FDFD simulations (blue dots). The straight red line indicates the maximal transmission cross section of an isotropic radiator. (b) Contour plot of the magnetic field intensity for the single slit excited at 0.676 μm shows strong excitation of the surface plasmon.

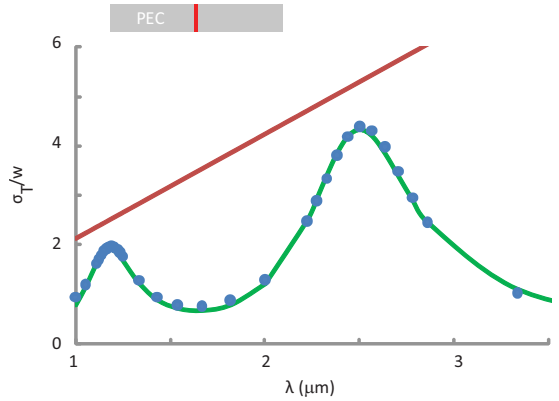

Fig. 7. (Color online) Single slit in a PEC, containing an absorbing material. The theoretical normalized transmission cross section spectrum (green curve) and from FDFD simulations (blue dots). The straight red line indicates the maximal transmission cross section of an isotropic radiator.

$$\sigma_T(\omega) = \frac{2\gamma_0 L\left(2\sum_{n=-N}^{N}\gamma_n\right)}{(\omega-\omega_0)^2+\left(2\sum_{n=-N}^{N}\gamma_n+\gamma_a\right)^2} = \frac{D\lambda_0}{\pi}\frac{\left(2\sum_{n=-N}^{N}\gamma_n\right)^2}{(\omega-\omega_0)^2+\left(2\sum_{n=-N}^{N}\gamma_n+\gamma_a\right)^2}. \quad (23)$$

Thus the presence of the loss reduces the peak transmission cross section.

As a numerical test of the theory, we simulate the transmission cross section of the same structure as shown in Fig. 3(a), except that the slit is now filled with a lossy dielectric with a refractive index of $1-0.02i$. In order to compare to the theory, we note that the absorption rate γ_a can be calculated approximately analytically as (Appendix B)

$$\gamma_a = \frac{cn_i k_0}{n_r}, \quad (24)$$

with n_r and n_i being the real and imaginary parts of the refractive index of the absorbing material inside the slit. Equation (24) provides a good first estimate of the absorption rate. All the other parameters of the theory are the same as the lossless slit. The result of the theory indeed agrees well with the direct numerical simulations (Fig. 7).

4. ABSORPTION CROSS SECTION

Photodetectors based on a resonant aperture have been shown to improve the signal/noise ratio [37], to help miniaturization [49], and to improve speed [50]. In these cases, the active semiconductor materials are placed in or around the apertures. The operation of devices relies upon achieving absorption cross sections that exceed the geometrical cross section of the aperture. Understanding the behavior of the absorption cross section in these systems is therefore crucial.

Here we use the slit to illustrate the temporal CMT formalism as applied to the design consideration of this type of photodetector. We consider an absorbing material in the slit and the bottom of the slit closed off with a PEC (Fig. 8, inset). The absorption cross section is defined as

$$\sigma_A(\omega) = \frac{P_A(\omega)}{F_{\text{inc}}(\omega)}, \quad (25)$$

with P_A being the absorbed power. In the absence of channels below the film, the absorption cross section for the detector, excited from the top with normally incident light, is derived as

$$\sigma_A(\omega) = \frac{4\gamma_a\gamma_0 L}{(\omega-\omega_0)^2+\left(\sum_{n=-N}^{N}\gamma_n+\gamma_a\right)^2} = \frac{D\lambda_0}{\pi}\frac{2\gamma_a\left(2\sum_{n=-N}^{N}\gamma_n\right)}{(\omega-\omega_0)^2+\left(\sum_{n=-N}^{N}\gamma_n+\gamma_a\right)^2}. \quad (26)$$

Under the critical coupling condition

$$\sum_{n=-N}^{N}\gamma_n = \gamma_a, \quad (27)$$

the resonant absorption cross section is maximized as

$$\sigma_A(\omega_0) = \frac{D\lambda_0}{\pi}. \quad (28)$$

Our theory thus indicates that the absorption cross section can be maximized by reaching the critical coupling condition and by enhancing the directivity of the aperture.

As a simple numerical illustration of the effect of critical coupling, we calculate the absorption cross section of the same (approximately isotropically radiating) slit in a PEC, closed off at the bottom and filled with a lossy di-

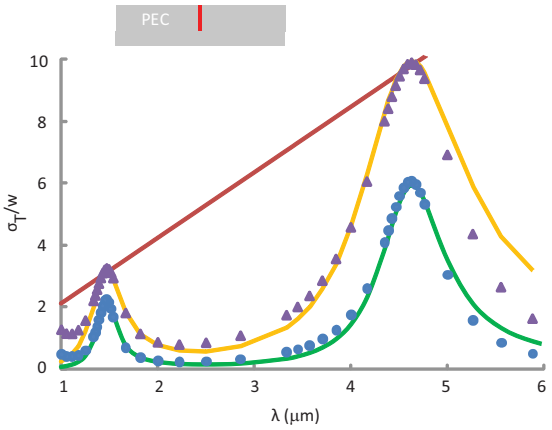

Fig. 8. (Color online) Absorption cross section of the slit. The theoretical normalized absorption cross section (green curve) and from FDFD simulations (blue dots) for non-critical coupling and for critical coupling (orange curve with purple triangles). The straight red line indicates the maximal absorption cross section of an isotropic radiator.

electric material (Fig. 8). When the lossy dielectric has an index of $1-0.02i$, the structure is not critically coupled, as is evident from the fact that the absorption cross section on resonance (lower curve) lies below the isotropic limit, indicated by the straight red line. By increasing the absorption in the material (refractive index $1-0.072i$), critical coupling can be achieved, leading to maximized absorption at the resonant frequency, as demonstrated by the upper curve. Further increasing the absorption loss beyond the critical coupling condition, however, leads to a degradation of the resonant absorption cross section. Thus, in optimizing aperture-based photodetectors, one cannot simply use the material with the highest absorption coefficient.

5. DISCUSSION AND CONCLUSIONS

We presented the derivation of the transmission cross section of a resonant aperture that couples two half-spaces based on the temporal coupled-mode theory (CMT). Our theory incorporates the effects of directivity, surface plasmon excitation, and material loss. The theory indicates that for an isotropic aperture, its maximum transmission cross section is independent of the geometry of the aperture, but instead only depends on the wavelength. Our theory also shows that the transmission cross section can be increased by enhancing the directivity. We have also applied our theory toward the absorption cross section of aperture-enhanced photodetectors and derived a critical coupling condition that maximizes the performance of such a detector.

Our formalism constitutes a reformulation of antenna theory and capture cross sections, in terms of a single resonant element. In antenna theory, the slit would have been considered as an aperture antenna coupled to a similar antenna through a transmission line. A transmission or absorption cross section is maximized when the antenna load is matched. For transmission, this can be achieved when the aperture antenna at the other side of the transmission line is identical; for absorption, as we demonstrated, this requires a specific refractive index for the material inside the slit. We believe that our formalism is more general—it only relies upon the existence of a resonance in the system and therefore is applicable to cases where the description of the transmission line is not immediately apparent, such as many optical antenna structures [51–54].

APPENDIX A: THREE-DIMENSIONAL CASE

Consider the case of a resonant aperture of finite extent in both x and y directions in a film of finite thickness in the z direction. The transmission, in the absence of loss or surface plasmons, is

$$T(\omega)=\frac{\sum_{m,n=-N}^{N}|s_{m,n-}|^2}{|s_{0,0+}|^2}=\frac{2\gamma_{0,0}\left(2\sum_{m,n=-N}^{N}\gamma_{m,n}\right)}{(\omega-\omega_0)^2+\left(2\sum_{m,n=-N}^{N}\gamma_{m,n}\right)^2}, \tag{A1}$$

where we now have a periodic boundary condition in both x and y directions and, consequently, discretization in both k_x and k_y, resulting in $(2N+1)^2$ channels, with indices m and n. The following identity holds for the isotropic radiator:

$$\sum_{m,n=-N}^{N}\gamma_{m,n}=\gamma_{0,0}\sum_{m,n=-N}^{N}\frac{1}{\cos\theta_n\cos\theta_m}=2N^2\pi\gamma_{0,0}, \tag{A2}$$

and the transmission cross section is derived as

$$\begin{aligned}\sigma_{T,\text{isotropic}}(\omega)&=\frac{2\gamma_{0,0}L^2\left(2\sum_{m,n=-N}^{N}\gamma_{m,n}\right)}{(\omega-\omega_0)^2+\left(2\sum_{m,n=-N}^{N}\gamma_{m,n}\right)^2}\\&=\frac{\frac{L^2}{2N^2\pi}\left(2\sum_{m,n=-N}^{N}\gamma_{m,n}\right)^2}{(\omega-\omega_0)^2+\left(2\sum_{m,n=-N}^{N}\gamma_{m,n}\right)^2}\\&=\frac{\lambda_0^2}{2\pi}\frac{\frac{1}{4Q^2}}{\left(\frac{\omega-\omega_0}{\omega_0}\right)^2+\frac{1}{4Q^2}}.\end{aligned} \tag{A3}$$

The transmission cross section for the isotropic radiator on resonance is then

$$\sigma_{T,\text{isotropic}}(\omega_0)=\frac{\lambda_0^2}{2\pi}. \tag{A4}$$

In general, however, the radiator in three dimensions will be directional. A small cylindrical hole, with propagating mode [10], or a small rectangular hole [14,15] excited by a plane wave will have more of a dipole character. A dipole that is significantly shorter than the wavelength has a directivity equal to 1.5. Consequently, the transmission cross section of such an aperture will be approximately $3\lambda_0^2/(4\pi)$. For an optically thick film, the transmission cross section will be a strong signature of the presence or absence of the propagating mode. Surface plasmon channels and absorption can be included in a similar way as described for the two-dimensional case.

APPENDIX B: ABSORPTION RATE

The absorption rate γ_a can be found by considering bulk material with refractive index $n=n_r-n_i i$. The exponential decay over the time it takes to travel an arbitrary distance Δ equals the exponential decay as a function of position:

$$\exp\left(\frac{-2\gamma_a n_r\Delta}{c}\right)=\exp(-2n_i k_0\Delta), \tag{B1}$$

and the absorption loss rate is

$$\gamma_a=\frac{cn_i k_0}{n_r}. \tag{B2}$$

ACKNOWLEDGMENTS

The authors thank Z. C. Ruan for helpful discussions. This research was supported by the MARCO Interconnect Focus Center.

REFERENCES AND NOTES

1. C. F. Bohren and D. R. Huffman, *Absorption and Scattering of Light by Small Particles* (Wiley, 1983).
2. K. L. Kelly, E. Coronado, L. Zhao, and G. C. Schatz, "The optical properties of metal nanoparticles: The influence of size, shape, and dielectric environment," J. Phys. Chem. B **107**, 668–677 (2003).
3. A. Arbouet, D. Christofilos, N. Del Fatti, F. Vallée, J. R. Huntzinger, L. Arnaud, P. Billaud, and M. Broyer, "Direct measurement of the single-metal-cluster optical absorption," Phys. Rev. Lett. **93**, 127401 (2004).
4. O. Muskens, N. Del Fatti, F. Vallee, J. R. Huntzinger, P. Billaud, and M. Boyer, "Single metal nanoparticle absorption spectroscopy and optical characterization," Appl. Phys. Lett. **88**, 063109 (2006).
5. M. Husnik, M. W. Klein, N. Feth, M. König, J. Niegemann, K. Busch, S. Linden, and M. Wegener, "Absolute extinction cross-section of individual magnetic split-ring resonators," Nat. Photonics **2**, 614–617 (2008).
6. J. A. Schuller and M. L. Brongersma, "General properties of dielectric optical antennas," Opt. Express **17**, 24084–24095 (2009).
7. T. W. Ebbesen, H. J. Lezec, H. F. Ghaemi, T. Thio, and P. A. Wolff, "Extraordinary optical transmission through subwavelength hole arrays," Nature **391**, 667–669 (1998).
8. C. Genet and T. W. Ebbesen, "Light in tiny holes," Nature **445**, 39–46 (2007).
9. S. Blair and A. Nahata, "Focus issue: Extraordinary light transmission through subwavelength structured surfaces—Introduction," Opt. Express **12**, 3618 (2004).
10. P. B. Catrysse and S. Fan, "Propagating plasmonic mode in nanoscale apertures and its implications for extraordinary transmission," J. Nanophotonics **2**, 021790 (2008).
11. F. J. García-Vidal, H. J. Lezec, T. W. Ebbesen, and L. Martín-Moreno, "Multiple paths to enhance optical transmission through a single subwavelength slit," Phys. Rev. Lett. **90**, 213901 (2003).
12. F. J. García de Abajo, "Light transmission through a single cylindrical hole in a metallic film," Opt. Express **10**, 1475–1484 (2002).
13. X. Shi, L. Hesselink, and L. R. Thornton, "Ultrahigh light transmission through a C-shaped nanoaperture," Opt. Lett. **28**, 1320–1322 (2003).
14. F. J. García-Vidal, E. Moreno, J. A. Porto, and L. Martín-Moreno, "Transmission of light through a single rectangular hole," Phys. Rev. Lett. **95**, 103901 (2005).
15. F. J. García-Vidal, L. Martín-Moreno, E. Moreno, L. K. S. Kumar, and R. Gordon, "Transmission of light through a single rectangular hole in a real metal," Phys. Rev. B **74**, 153411 (2006).
16. T. Thio, K. M. Pellerin, R. A. Linke, H. J. Lezec, and T. W. Ebbesen, "Enhanced light transmission through a single subwavelength aperture," Opt. Lett. **26**, 1972–1974 (2001).
17. H. A. Haus, *Waves and Fields in Optoelectronics* (Prentice-Hall, 1984).
18. R. E. Hamam, A. Karalis, J. D. Joannopoulos, and M. Soljacic, "Coupled-mode theory for general free-space resonant scattering of waves," Phys. Rev. A **75**, 053801 (2007).
19. Z. Ruan and S. Fan, "Temporal coupled-mode theory for Fano resonance in light scattering by a single obstacle," J. Phys. Chem. C **114**, 7324–7329 (2010).
20. J. Bravo-Abad, L. Martín-Moreno, and F. J. García-Vidal, "Transmission properties of a single metallic slit: From the subwavelength regime to the geometrical-optics limit," Phys. Rev. E **69**, 026601 (2004).
21. O. Mata-Mendez and J. Avendaño, "Some properties of the optical resonances in a single subwavelength slit," J. Opt. Soc. Am. A **24**, 1687–1694 (2007).
22. F. Yang and J. R. Sambles, "Resonant transmission of microwaves through a narrow metallic slit," Phys. Rev. Lett. **89**, 063901 (2002).
23. Y. Takakura, "Optical resonance in a narrow slit in a thick metallic screen," Phys. Rev. Lett. **86**, 5601–5603 (2001).
24. J. R. Suckling, A. P. Hibbins, M. J. Lockyear, T. W. Preist, J. R. Sambles, and C. R. Lawrence, "Finite conductance governs the resonance transmission of thin metal slits at microwave frequencies," Phys. Rev. Lett. **92**, 147401 (2004).
25. R. Gordon, "Light in a subwavelength slit in a metal: Propagation and reflection," Phys. Rev. B **73**, 153405 (2006).
26. P. Lalanne, J. P. Hugonin, and J. C. Rodier, "Theory of surface plasmon generation at nanoslit apertures," Phys. Rev. Lett. **95**, 263902 (2005).
27. L. Martín-Moreno, F. J. García-Vidal, H. J. Lezec, A. Degiron, and T. W. Ebbesen, "Theory of highly directional emission from a single subwavelength aperture surrounded by surface corrugations," Phys. Rev. Lett. **90**, 167401 (2003).
28. Q. Min and R. Gordon, "Surface plasmon microcavity for resonant transmission through a slit in a gold film," Opt. Express **16**, 9708–9713 (2008).
29. Z. C. Ruan and M. Qiu, "Enhanced transmission through periodic arrays of subwavelength holes: The role of localized waveguide resonances," Phys. Rev. Lett. **96**, 233901 (2006).
30. F. J. García-Vidal, L. Martín-Moreno, H. J. Lezec, and T. W. Ebbesen, "Focusing light with a single subwavelength aperture flanked by surface corrugations," Appl. Phys. Lett. **83**, 4500–4502 (2003).
31. Z. Sun and H. K. Kim, "Refractive transmission of light and beam shaping with metallic nano-optic lenses," Appl. Phys. Lett. **85**, 642–644 (2004).
32. H. Shi, C. Wang, C. Du, X. Luo, X. Dong, and H. Gao, "Beam manipulating by metallic nano-slits with variant widths," Opt. Express **13**, 6815–6820 (2005).
33. L. Verslegers, P. B. Catrysse, Z. Yu, J. S. White, E. Barnard, M. L. Brongersma, and S. Fan, "Planar lenses based on nano-scale slit arrays in a metallic film," Nano Lett. **9**, 235–238 (2009).
34. L. Verslegers, P. B. Catrysse, Z. Yu, and S. Fan, "Planar metallic nanoscale slit lenses for angle compensation," Appl. Phys. Lett. **95**, 071112 (2009).
35. L. Verslegers, P. B. Catrysse, Z. Yu, W. Shin, Z. C. Ruan, and S. Fan, "Phase front design with metallic pillar arrays," Opt. Lett. **35**, 844–846 (2010).
36. L. Verslegers, P. B. Catrysse, Z. Yu, and S. Fan, "Deep-subwavelength focusing and steering of light in an aperiodic metallic waveguide array," Phys. Rev. Lett. **103**, 033902 (2009).
37. Z. Yu, G. Veronis, S. Fan, and M. L. Brongersma, "Design of midinfrared photodetectors enhanced by surface plasmons on grating structures," Appl. Phys. Lett. **89**, 151116 (2006).
38. J. S. White, G. Veronis, Z. Yu, E. S. Barnard, A. Chandran, S. Fan, and M. L. Brongersma, "Extraordinary optical absorption through sub-wavelength slits," Opt. Lett. **34**, 686–688 (2009).
39. W. L. Stutzman and G. A. Thiele, *Antenna Theory and Design*, 2nd ed. (Wiley, 1998).
40. S. Drabowitch, A. Papiernik, H. Griffiths, J. Encinas, and B. L. Smith, *Modern Antennas* (Chapman & Hall, 1998).
41. A. Alu and N. Engheta, "Tuning the scattering response of optical nanoantennas with nanocircuit loads," Nat. Photonics **2**, 307–310 (2008).
42. Z. Yu, A. Raman, and S. Fan, "Fundamental limit of nanophotonic light trapping for solar cells," for Proc. Natl. Acad. Sci. (to be published).
43. S. Fan, W. Suh, and J. D. Joannopoulos, "Temporal coupled mode theory for Fano resonances in optical resonators," J. Opt. Soc. Am. A **20**, 569–573 (2003).
44. J. B. Keller, "Geometrical theory of diffraction," J. Opt. Soc. Am. **52**, 116–130 (1962).
45. G. Veronis and S. Fan, in *Surface Plasmon Nanophotonics*, M. L. Brongersma and P. G. Kik, eds. (Springer, 2007), p. 169.
46. The directivity, as we defined it, is analogous to the direc-

tivity in antenna theory, defined as the ratio of $U(\theta)$, the radiation intensity in a certain direction, to U_{ave}, the average radiation intensity: $D(\theta)=U(\theta)/U_{ave}$ (two-dimensional case).
47. The factor G is called the (power) gain in antenna theory [39]. We do not adopt this name since in the optics literature gain is commonly related to amplification, which is not the case here.
48. D. R. Lide, ed., *CRC Handbook of Chemistry and Physics*, 88th ed. (CRC, 2007).
49. L. Tang, D. A. B. Miller, A. K. Okyay, J. A. Matteo, Y. Yuen, K. C. Saraswat, and L. Hesselink, "C-shaped nanoaperture-enhanced germanium photodetector," Opt. Lett. **31**, 1519–1521 (2006).
50. L. Tang, S. E. Kocabas, S. Latif, A. K. Okyay, D.-S. Ly-Gagnon, K. C. Saraswat, and D. A. B. Miller, "Nanometer-scale germanium photodetector enhanced by a near-infrared dipole antenna," Nat. Photonics **2**, 226–229 (2008).
51. P. Bharadwaj, B. Deutsch, and L. Novotny, "Optical antennas," Adv. Opt. Photon. **1**, 438–483 (2009).
52. K. B. Crozier, A. Sundaramurthy, G. S. Kino, and C. F. Quate, "Optical antennas: Resonators for local field enhancement," J. Appl. Phys. **94**, 4632–4642 (2003).
53. P. Muhlschlegel, H. J. Eisler, O. J. F. Martin, B. Hecht, and D. W. Pohl, "Resonant optical antennas," Science **308**, 1607–1609 (2005).
54. A. Kinkhabwala, Z. Yu, S. Fan, Y. Avlasevich, K. Mullen, and W. E. Moerner, "Single-molecule fluorescence enhancements produced by a Bowtie nanoantenna," Nat. Photonics **3**, 654–657 (2009).